RSC Advances

PAPER

View Article Online
View Journal | View Issue

Cite this: *RSC Adv.*, 2014, **4**, 15914

Ultra-fast photonic curing of electrically conductive adhesives fabricated from vinyl ester resin and silver micro-flakes for printed electronics†

Hui-Wang Cui,*[a] Jin-Ting Jiu,[a] Shijo Nagao,[a] Tohru Sugahara,[a] Katsuaki Suganuma,[a] Hiroshi Uchida[b] and Kurt A. Schroder[c]

Received 11th January 2014
Accepted 6th February 2014

DOI: 10.1039/c4ra00292j

www.rsc.org/advances

To avoid high temperatures and long curing times, both of which are impractical in the manufacture of flexible printed electronic devices, we fabricated new electrically conductive adhesives using vinyl ester resin and silver micro-flakes and introduced an intense pulse of light to cure the adhesives under an ambient atmosphere at room temperature. The electrically conductive vinyl ester resin–silver micro-flake adhesives can absorb intense pulsed light, which initializes the double bonds in the resin to successfully achieve crosslinking and curing. This curing process, known as photonic curing, can be completed within a second under an ambient atmosphere at room temperature, over a large area. A typical curing time was 140 ms without any photosensitizers or photoinitiators in the adhesives. The cured conductive adhesives had low bulk resistivity, *e.g.*, 7.54×10^{-6} Ω cm and high bonding strength, *e.g.*, 6.75 MPa. Thus, the combination of photonic curing and electrically conductive vinyl ester resin–silver micro-flake adhesives has great potential for printed electronics, which require low temperature and fast processes based on flexible devices.

Introduction

As an environmentally friendly alternative to lead-bearing solders, electrically conductive adhesives (ECAs) have been used widely in the manufacture of microelectronics because of the reduced number of processing steps (*e.g.*, elimination of fluxing and reduction of cleaning components), low processing temperatures, which enable the use of heat-sensitive and low cost components and substrates, and potentially enables fine pitch interconnections.[1,2] Improving mechanical strength, increasing electrical conductivity, shortening curing time, raising production efficiency, *etc.*, have been hot research topics for the development and application of ECAs.[2] Copper particles,[3,4] silver micro-flakes,[5,6] silver nanorods,[7,8] functionalized carbon nanotubes,[9–11] silver plated graphite nanosheets,[12,13] silver nanowires,[14,15] and hexagonal boron nitride nanoparticles[16,17] have been used as electrically conductive fillers to increase electrical conductivity. Epoxy,[10,11] silicone resin,[18,19] polyimide resin,[20,21] phenol–formaldehyde resin,[22,23] polyurethane,[24,25] and acrylic resin[26,27] together with diluents,[6,28] curing agents,[6,28] crosslinkers,[29,30] coupling agents,[6,28] preservatives,[31,32] toughening agents,[33,34] thixotropic agents,[35] photosensitizers and photoinitiators[36,37] have been used as matrix resins to improve mechanical strength and shorten curing time. Most of these ECAs are cured by heat at 120–150 °C in 30–60 min or by ultraviolet rays in several to tens of minutes. However, the heat and ultraviolet ray curing conditions, due to the limitations of high temperatures and long curing times, are unacceptable if ECAs are to be used in printed electronics, which need low temperatures and short processing times.

For printed electronics, many high-speed sintering systems, such as electrical,[38,39] laser,[40,41] microwave,[42,43] and photonic curing,[44,45] also refereed to as flash light[46,47] or intense pulsed light,[48–50] have been developed to replace conventional heat sintering processes which take between a few minutes to a few hours. Among them, the photonic curing technique can sinter and cure materials in an ambient atmosphere over a large area almost instantly – from microseconds to a few seconds. This technique plays an important role in roll-to-roll printing processes of rapid and eco-friendly electronic device manufacturing and can achieve higher throughput than any other sintering technique in printed electronics. So far there are no reports on using photonic curing to cure ECAs because heat curing and ultraviolet ray curing are still the mainstream

[a]*Institute of Scientific and Industrial Research, Osaka University, Mihogaoka 8-1, Ibaraki, Osaka 567, Japan. E-mail: cuihuiwang@eco.sanken.osaka-u.ac.jp; cuihuiwang@hotmail.com*

[b]*Institute for Polymers and Chemicals Business Development Center, Showa Denko K. K., 5-1 Yawata Kaigan Dori, Ichihara, Chiba 290-0067, Japan*

[c]*NCC Nano, LLC, 200-B Parker Drive, Suite 580, Austin, TX 78728, USA*

† Electronic supplementary information (ESI) available: Diagrams and UV-Vis-NIR spectra. See DOI: 10.1039/c4ra00292j

methods for the application of ECAs. Therefore, in this study, we fabricated ECAs using a vinyl ester resin and silver micro-flakes, and then introduced an intense pulsed light to cure them (Scheme 1). We investigated the curing, thermal, electrical and mechanical properties, and surface morphologies using Fourier transform infrared spectroscopy (FTIR), differential scanning calorimetry (DSC), thermogravimetric-differential thermal analysis (TG-DTA), field emission scanning electron microscopy (FE-SEM), a four-point probe method, nanoindentation, and a shear test.

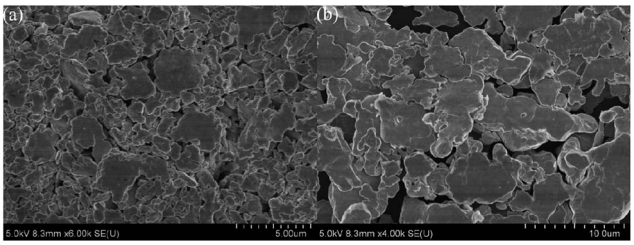

Fig. 1 Surface morphologies of (a) AgC-239 and (b) AgC-224 silver micro-flakes.

Experiments

Samples

The ECAs consisted of a matrix resin and electrically conductive fillers. The matrix resin was a Ripoxy SP-1507 vinyl ester resin from Showa Denko, Chibaken, Japan, which was a bisphenol A epoxy acrylate diluted by ethoxylated bisphenol A diacrylate [Scheme 1(a)]. The viscosity was 18 700 mPa s (25 °C). The electrically conductive fillers were AgC-239 silver micro-flakes [Fig. 1(a)] from Fukuda Metal Foil & Powder Co., Ltd., Kyoto, Japan. The size of the micro-flakes was 2–15 μm and the thickness around 0.5 μm. The weight percentages of the silver micro-flakes in the ECAs were 80%, 85%, and 90%. The ECAs were named ECA-80, ECA-85, and ECA-90 accordingly. To fabricate these ECAs, silver micro-flakes were incorporated into the vinyl ester resin using a THINKY ARV-310 planetary vacuum mixer (THINKY Corporation, Laguna Hills, CA, USA) under 2000 rpm for 20 min [Scheme 1(a)]. After fabrication, the ECAs were stored at room temperature for further use. To conduct the photonic curing, the ECAs were printed onto glass substrates [Scheme 1(b)], and were then irradiated and sintered using a commercial photonic curing system (PulseForge® 3300, Novacentrix, Austin, TX, USA.) [Scheme 1(c) and (d)]. This process was performed under an ambient atmosphere at room temperature. Typical input parameters were voltage (220 V) and pulse duration (1400 μs). The measured radiant exposure energy for each pulse was 2.4 J cm^{-2}. Different numbers of pulses were applied to cure the ECAs. The repetition rate was 3 Hz.

Characterization

The structures of the samples were recorded using a PerkinElmer Frontier TN FTIR spectrophotometer (PerkinElmer, Waltham, MA, USA); 32 scans were collected at a spectral resolution of 1 cm^{-1}. The curing of the samples was studied using a NETZSCH 204 F1 DSC calorimeter (NETZSCH, Selb, Germany) operated under a pure Ar atmosphere. The sample (*ca.* 10 mg) was placed in a sealed aluminium sample pan. The

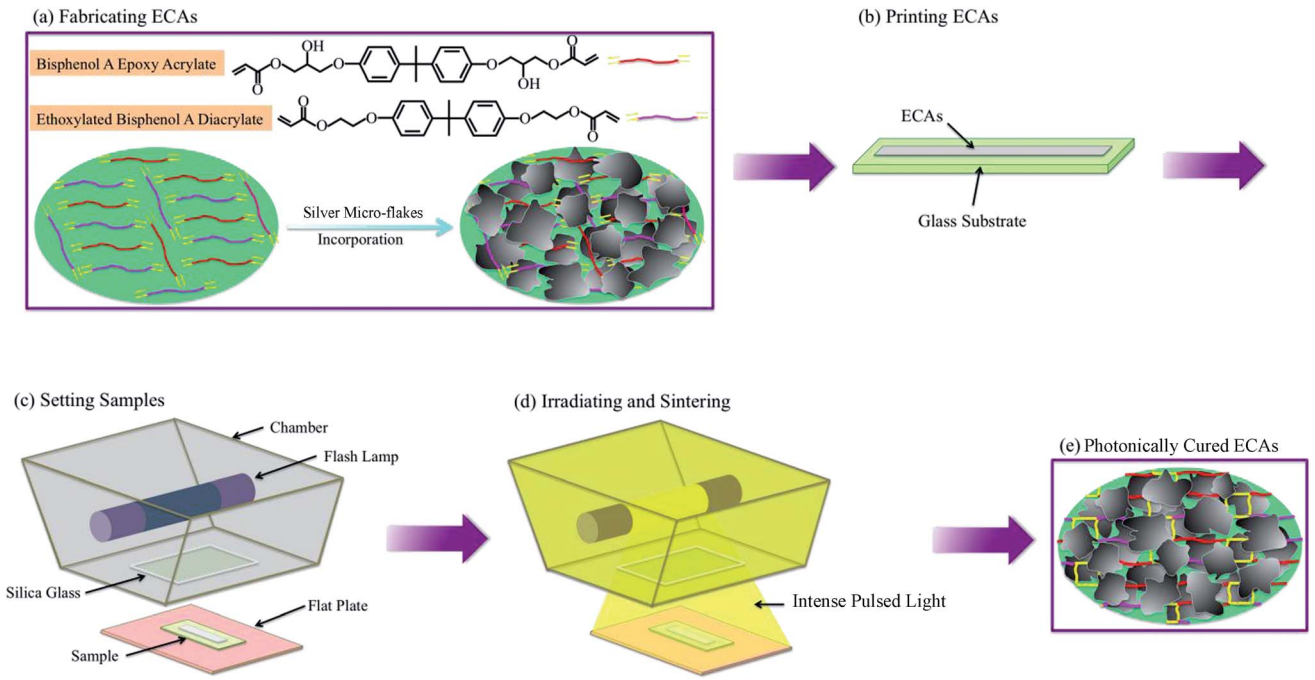

Scheme 1 Preparation of ultra-fast photonically cured ECAs: (a) fabricating ECAs, (b) printing ECAs, (c) setting samples, (d) irradiating and sintering, and (e) photonically cured ECAs.

curing scans were conducted from 40 to 300 °C at a rate of 10 °C min^{-1} under an Ar flow rate of 25 ml min^{-1}. The thermal stabilities of the samples were measured using a NETZSCH 2000SE/H/24/1 TG-DTA analyzer (NETZSCH, Selb, Germany) operated under a pure N_2 atmosphere. The sample (*ca.* 10 mg) was placed in a Pt cell and heated at a rate of 10 °C min^{-1} from 30 to 900 °C under a N_2 flow rate of 60 ml min^{-1}. SEM images of the samples were recorded using a Hitachi SU8020 FE-SEM microscope (Hitachi, Tokyo, Japan) operated at an accelerating voltage of 5 kV and an accelerating current of 2 μA. The bulk resistivity of the samples was obtained using a Loresta-GP MCP-T610 resistivity meter (Mitsubishi Chemical Analytech, Co., Ltd., Kanagawa, Japan) through a four-point probe method. The tested samples were prepared according to Fig. S1.† The ECAs were printed onto a glass substrate (50 mm × 10 mm × 1 mm) with the help of a glue tape (thickness 50 μm, 3M, Maplewood, MN, USA) to form ECA films (30 mm × 5 mm × 0.05 mm). 30 samples were tested for each value. The shear strength of the samples was measured using a Nordson Dage Series 4000 multipurpose bond tester (Nordson, Westlake, OH, USA) through a DS 100 kg SK Chipshear model. The tested samples were prepared according to Fig. S2.† The printed ECA film (5 mm × 5 mm × 0.05 mm) on a glass substrate (5 mm × 5 mm × 1 mm) was connected to another glass chip (5 mm × 5 mm × 1 mm) to form a sandwich structure. The width of the pusher head was 4 mm. The push rate was 100 μm s^{-1}. 30 samples were tested for each value. The optical absorption of the samples was measured using a JASCO V-670 UV-Vis-NIR spectrophotometer (JASCO Corporation, Tokyo, Japan) in the range of 200–900 nm. The nano-dynamic mechanical properties of the samples were obtained using a Hysitron TI 950 TriboIndenter (HYSITRON, Eden Prairie, MN, USA) under a scanning rate of 0.5 Hz, a tip velocity of 40 μm s^{-1}, a scanning size of 40 μm, a setpoint of 3 μN, and an integral grain of 120.

Results and discussion

Curing

We used FTIR to characterize the structure of ECA-80. As indicated by the arrows in Fig. 2, the strong sharp absorption peak at 1720 cm^{-1} featured the stretching vibration of C=O, the weak absorption peak at 1635 cm^{-1} was due to the stretching vibration of C=C in alkenyl, the peak at 1415 cm^{-1} was due to the in-plane bending vibration of C–H in the alkenyl groups, and the peaks at 985 and 805 cm^{-1} were for the out-plane bending vibration of C–H in alkenyl. The cured and uncured ECA-80 both contained these groups.

In this study, the matrix resin and silver micro-flakes showed excellent light-absorbing properties. Both presented strong, sharp absorption peaks at wavelengths of 200–300 nm on the UV-Vis-NIR spectra (Fig. S3†). Under intense pulsed light, ECA-80 absorbed the heat produced from the light, which was then transferred to the whole matrix resin system. During this transfer, the heat opened the double bonds at the end of molecular chains and caused crosslinking to accomplish the curing process. During irradiation and sintering, the temperature caused by the intense pulsed light could be up to 200 °C, which accelerated the opening and crosslinking processes. Therefore, the intense pulsed light, combined with a high radiant exposure energy (2.38 J cm^{-2}) and a long pulse duration (1400 μs), had given enough activation energy to the matrix resin and opened the double end bonds to initialize crosslinking, polymerization, and curing[49–51] [Scheme 1(d)–(e)].

As the number of light pulses increased from 5 to 300 pulses, the absorption peaks at 1635, 1415, 985, and 805 cm^{-1}, which represented the characteristics of alkenyl groups in the matrix resin, became weak, and ultimately disappeared. These variations indicated the conversion process of double bonds during curing. The double bond conversion can be calculated using the following equation:[52–54]

$$\text{Conversion} = 1 - \left(\frac{A^{t}_{C=C}A^{0}_{C=O}}{A^{0}_{C=C}A^{t}_{C=O}}\right) \times 100$$

where $A^{0}_{C=C}$ is the area of the C=C absorption peaks of uncured samples, $A^{t}_{C=C}$ is the area of the C=C absorption peaks of samples cured for a time of t, $A^{0}_{C=O}$ is the area of the C=O absorption peaks of uncured samples, and $A^{t}_{C=O}$ is the area of the C=O absorption peaks of samples cured for a time of t. In the above calculation, we used the areas of the C=O absorption peaks as references, because the C=O did not have any reactions during curing and often showed strong and sharp absorption peaks in the FTIR spectra.

Fig. 3 shows the double bond conversion of ECA-80 *vs.* curing time. They were 4.87% (5 pulses), 15.59% (20 pulses), 47.24% (40 pulses), 54.57% (50 pulses), 67.02% (60 pulses), 80.68% (80 pulses), 94.36% (100 pulses), 97.01% (200 pulses), and 99.38% (300 pulses), respectively. The double bond conversion increased sharply between 5 to 100 pulses, then showed a slow increasing trend between 200 to 300 pulses. This suggested that ECA-80 could be cured well at 100 pulses.

In addition, we also used DSC to characterize the curing degree of the photonic curing. As Fig. 4 shows, ECA-80, photonically cured at 100, 200, and 300 pulses, did not present any endothermic peaks within the testing temperatures (40–300 °C). This indicated that the ECAs were cured well at these pulses, corresponding to the curing times of 140, 280, and 420 ms, respectively, which also coincided well with the aforementioned FTIR results.

Fig. 5 displays the TG-DTA traces of the cured ECA-80, ECA-85, and ECA-90. As shown in Fig. 5(a), the TG traces revealed a loss of the matrix resin; the total weight loss was about 17% (ECA-80, 100 pulses), 14% (ECA-85, 100 pulses), 10% (ECA-90, 100 pulses), 8% (ECA-80, 500 pulses), 6% (ECA-85, 500 pulses), and 4% (ECA-90, 500 pulses) at the temperatures up to 900 °C. The weight loss increased quickly from about 350 to 450 °C, where the pyrolysis rate was the maximum. At temperatures higher than 450 °C, the weight loss was slow. The high pyrolysis temperature above 350 °C suggested that these ECAs all had high temperature stability. The weight losses of ECA-80, ECA-85, and ECA-90 at 500 pulses were less than those at 100 pulses. This is because the intense pulsed light produced too much

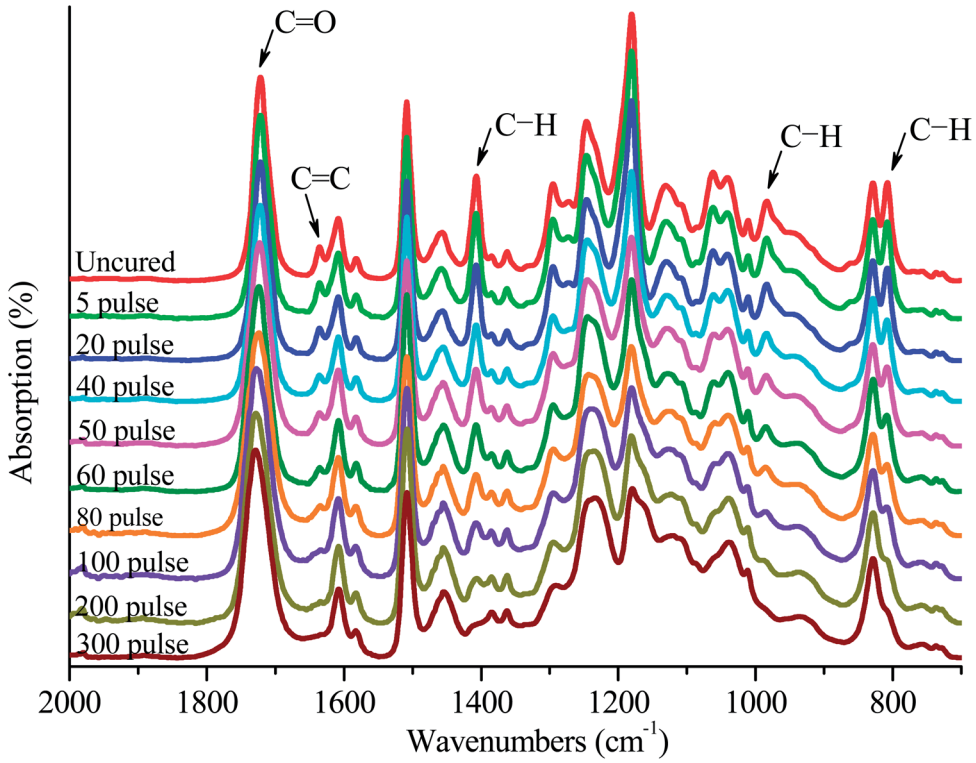

Fig. 2 FTIR spectra of ECA-80.

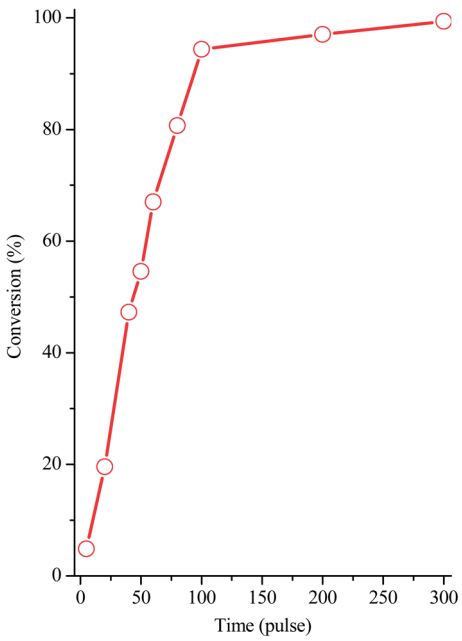

Fig. 3 Double bond conversion of ECA-80.

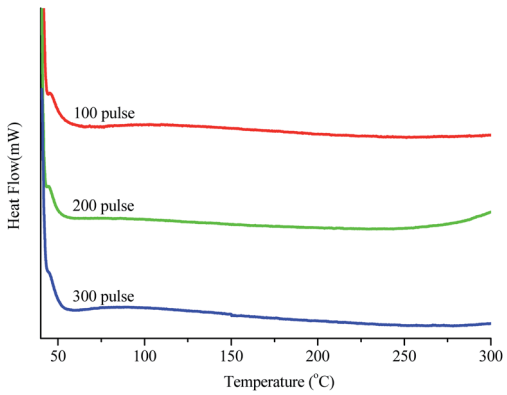

Fig. 4 DSC curves of the photonically cured ECA-80.

energy over a long curing time, which caused the pyrolysis of the matrix resin under an ambient atmosphere.

Fig. 5(b) shows the DTA traces of ECA-80, ECA-85, and ECA-90 at 100 and 500 pulses. They all had an endothermic peak in the range of 350–450 °C. The shape, intensity, and area of these endothermic peaks changed accordingly with the weight losses of ECA-80, ECA-85, and ECA-90. The higher the weight loss, the sharper, stronger, and larger the endothermic peak. At 100 pulses, the weight losses of ECA-80, ECA-85, and ECA-90 were approximately equal to the weight percentages of the matrix resin in them. From the weight loss and endothermic peaks, it can be seen that the ECAs achieved good curing with negligible pyrolysis of the matrix resin using 100 pulses irradiating and sintering energy with 140 ms under an ambient atmosphere. Compared to heat curing for 30–60 min at 120–150 °C, or curing with ultraviolet rays for several to tens of minutes, intense pulsed light curing was ultra-fast. Importantly, there was only one weight loss step and one endothermic peak for each ECA,

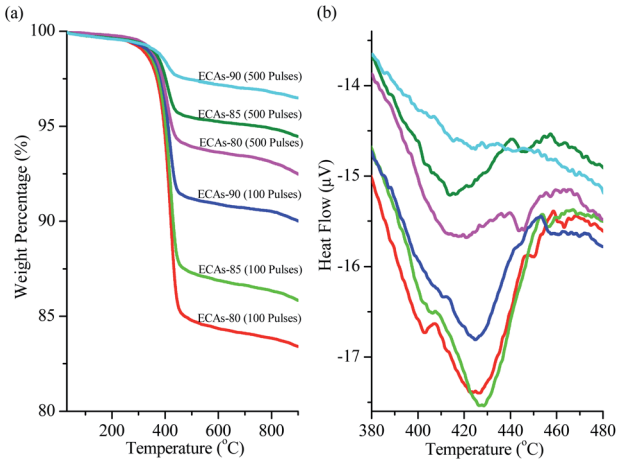

Fig. 5 TG-DTA traces of ECA-80, ECA-85, and ECA-90: (a) TG and (b) DTA traces.

which indicated that a crosslinked homogeneous polymer had been formed from the matrix resin by the intense pulsed light [Scheme 1(e)], with no residual monomers or small molecules. Combining the double bond conversion and weight loss, we set the curing time of the ECAs as 100 pulses in this study.

Electrical properties

The samples were prepared using 100 pulses for bulk resistivity (Fig. S1†). Besides AgC-239 silver micro-flakes, AgC-224 silver micro-flakes [Fig. 1(b), Fukuda Metal Foil & Powder Co., Ltd., Kyoto, Japan] were used to fabricate ECAs for comparison samples. Fig. 6 shows the bulk resistivity results. As the weight

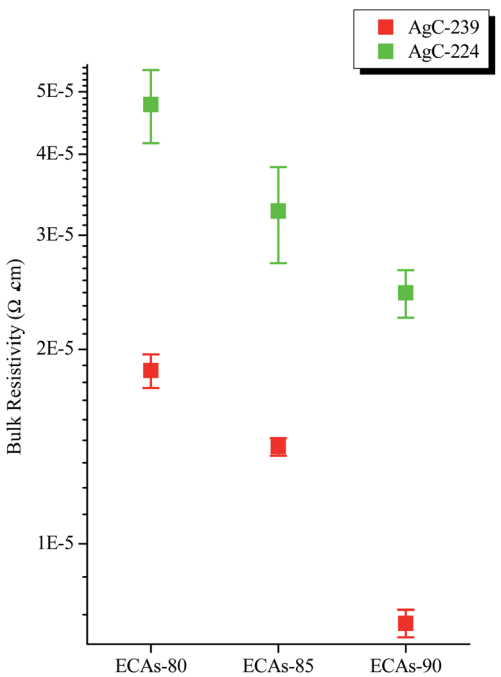

Fig. 6 Bulk resistivity of ECA-80, ECA-85, and ECA-90 at 100 pulses.

percentage of silver micro-flakes increased from 80% to 90% in the ECAs, the bulk resistivity decreased accordingly.

Bulk resistivity has a close relationship to the content of the electrically conductive fillers; the higher the content of electrically conductive fillers, the lower the bulk resistivity. This is because the increasing electrically conductive fillers form more electrically conductive channels, which decrease the bulk resistivity. AgC-239 silver micro-flakes had a more significant effect on decreasing bulk resistivity than the AgC-224 silver micro-flakes. As shown in Fig. 6, the bulk resistivity was 1.85×10^{-5}, 1.41×10^{-5}, and 7.54×10^{-6} Ω cm, respectively, for ECA-80, ECA-85, and ECA-90 fabricated from AgC-239 silver micro-flakes, and 4.78×10^{-5}, 3.27×10^{-5} and 2.44×10^{-5} Ω cm for those fabricated from AgC-224 silver micro-flakes. In addition, the bulk resistivity values for AgC-239 silver micro-flakes were also much lower than those at 3×10^{-5} to 5×10^{-5} Ω cm in our previous studies.[6,10,11,16,17]

The formation of electrically conductive channels (also called electrically conductive networks) in the ECAs mainly came from the contact points and areas between/among electrically conductive fillers; the greater the number of contact points, the larger the contact area, and the higher the electrical conductivity. To obtain clear profiles of electrically conductive channels, ECA-90 from AgC-239 and AgC-224 silver micro-flakes was irradiated and sintered for 500 pulses. After this process, the matrix resin was pyrolysed almost completely; there were only silver micro-flakes left in the ECAs. Thus, the electrically conductive channels were formed by sintered structures [Fig. 7(a) and (b)]. The shape and size of the silver micro-flakes greatly influenced the formation of electrically conductive channels. AgC-239 silver micro-flakes had a size of 2–15 μm [Fig. 1(a)], and AgC-224 silver micro-flakes had a size of 6–12 μm [Fig. 1(b)], so that the former had a wider size distribution than the latter. Their shapes were also different.

As Fig. 7(a) shows, AgC-239 silver micro-flakes overlapped and contacted each other to form a dense and fine electrically conductive network. The interspaces and holes between/among the AgC-239 silver micro-flakes were caused by the pyrolysis of the matrix resin. They were very small. A similar electrically conductive network was also formed from the AgC-224 silver micro-flakes, but was sparse and rough [Fig. 7(b)]. Moreover, the interspaces and holes between/among the AgC-224 silver micro-flakes were very large. Fig. 7(c) shows the cross-sectional morphology of ECA-90 fabricated from the AgC-239 silver micro-flakes after 100 pulses. It can be seen that the AgC-239 silver micro-flakes were densely dispersed and arranged tightly in the matrix resin, while the morphology of ECA-90 fabricated from the AgC-224 silver micro-flakes did not look like this. As shown in Fig. 7(d), the AgC-224 silver micro-flakes were evenly dispersed in the matrix resin, but not as densely or tightly as the AgC-239 silver micro-flakes. Fig. 7(e) and (f) present the arrangement models of the AgC-239 and AgC-224 silver micro-flakes in ECA-90. The arrangement of the AgC-224 silver micro-flakes [Fig. 7(f)] had many large interspaces and holes, representing that these silver micro-flakes did not contact each other fully, and the electrically conductive channels were not well formed. Thus, the bulk resistivity showed high values. The

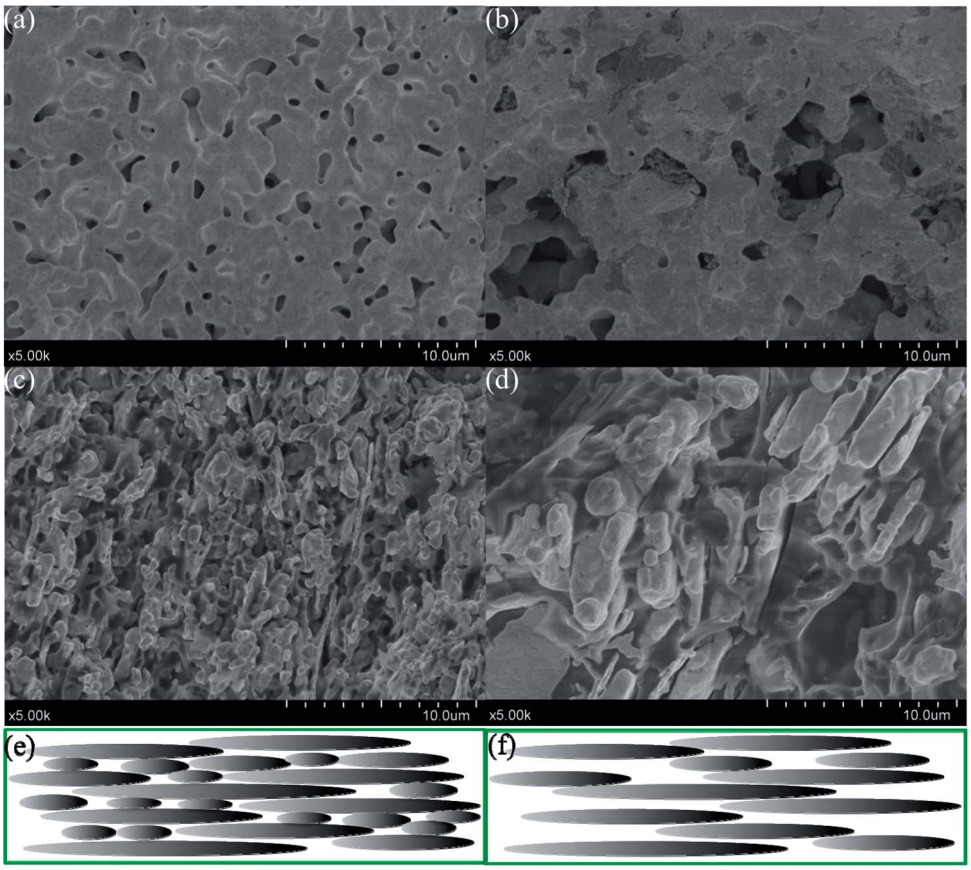

Fig. 7 Surface morphologies of the sintered structures of ECA-90 (500 pulses) fabricated with (a) AgC-239 and (b) AgC-224 silver micro-flakes, cross-sectional morphologies of ECA-90 (100 pulses) fabricated with (c) AgC-239 and (d) AgC-224 silver micro-flakes, and arrangement models of (e) AgC-239 and (f) AgC-224 silver micro-flakes in ECA-90.

arrangement of the AgC-239 silver micro-flakes was not like that of the AgC-224 silver micro-flakes [Fig. 7(e)]. Small silver micro-flakes were filled or embedded into the interspaces and holes formed by large ones, to produce many contact points and increase contact areas. Electrically conductive channels were well formed due to this arrangement, leading to low bulk resistivity.

Mechanical properties

To investigate the mechanical properties of the photonically cured ECAs, samples were designed for a shear test according to Fig. S2.† ECAs were printed onto a glass substrate, and then a glass chip was put on the ECA film to form a sandwich structure. As described above, the 0.05 mm thick ECA film was cured well by direct exposure to intense pulsed light for 100 pulses. During the preparation of the shear test samples, the intense pulsed light at 100 pulses could not cure the sandwiched ECA film entirely because the glass chip covered and weakened the light intensity greatly. To fully cure the ECA films in these samples, 500 pulses were used.

Fig. 8(a) presents the shear strength of ECA-80, ECA-85, and ECA-90 obtained from the shear test. These shear strength values at 6.75, 6.25, and 5.00 MPa were higher than some previously reported results at 4–11 MPa.[6,10,11,33,34] The intense

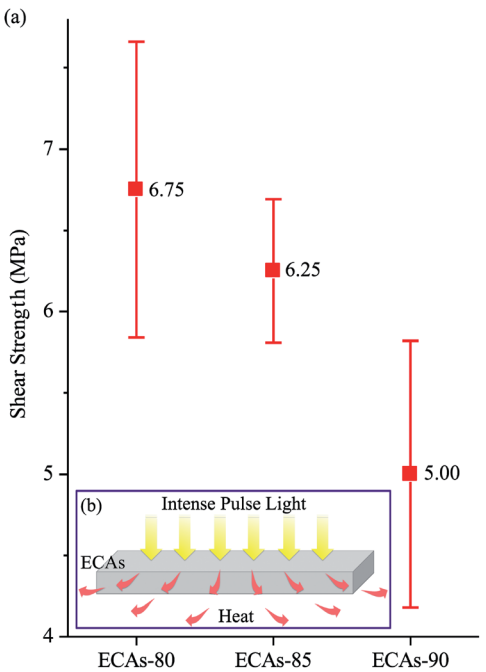

Fig. 8 (a) The shear strength of ECA-80, ECA-85, and ECA-90 from photonic curing (500 pulses) and (b) a light and heat transfer diagram.

pulsed light, combining a high bank voltage (220 V), long pulse duration (1400 μs), and high radiant exposure energy (2.38 J cm^{-2}), was used to cure these ECAs. The matrix resin and silver micro-flakes firstly absorbed the light and the heat produced from light, which were then transferred into the whole matrix resin system [Fig. 8(b)]. With the heat, the double bonds at the end of the molecular chains were initialized into crosslinking and polymerization, and then cured the ECAs as previously reported.[51–54] The process also caused the pyrolysis of the matrix resin and sintered silver micro-flakes together [Fig. 7(a) and (b)].

The matrix resin was connected *via* opened double bonds and crosslinked into macromolecules as reflected in the FTIR spectra. Moreover, the main molecular chains of the matrix resin contained hydroxyl, carbonyl, and epoxy groups. They were induced to form intermolecular hydrogen bonds [Fig. S4(a)†]. In addition, hydrogen bonds were also formed between AgC-239 silver micro-flakes and crosslinked macromolecules of bisphenol A epoxy acrylate [Fig. S4(b)†] and ethoxylated bisphenol A diacrylate [Fig. S4(c)†], because the coated fatty acid on the silver micro-flakes had these functional groups, too. In a word, good curing, sintered silver micro-flakes, and hydrogen bonds all contributed to the high shear strength of the photonically cured ECAs.

It can also be seen that the mechanical strength of the ECAs was reduced with increasing silver micro-flake content due to cutting off the crosslinked structures within the matrix resin. Fig. 9 presents the surface morphologies of pushed fracture interfaces on glass substrates and chips. The pushed fracture interfaces on glass substrates all looked flat. Those at ECA-80 had the most collapses and potholes [Fig. 9(a)], followed by ECA-85 [Fig. 9(c)], and finally, ECA-90 had few collapses and potholes [Fig. 9(e)]. The pushed fracture interfaces on glass chips were made up of torn particles, torn traces, collapses, and potholes, showing a decreasing rough state from ECA-80 [Fig. 9(b)] to ECA-85 [Fig. 9(d)], and to ECA-90 [Fig. 9(f)].

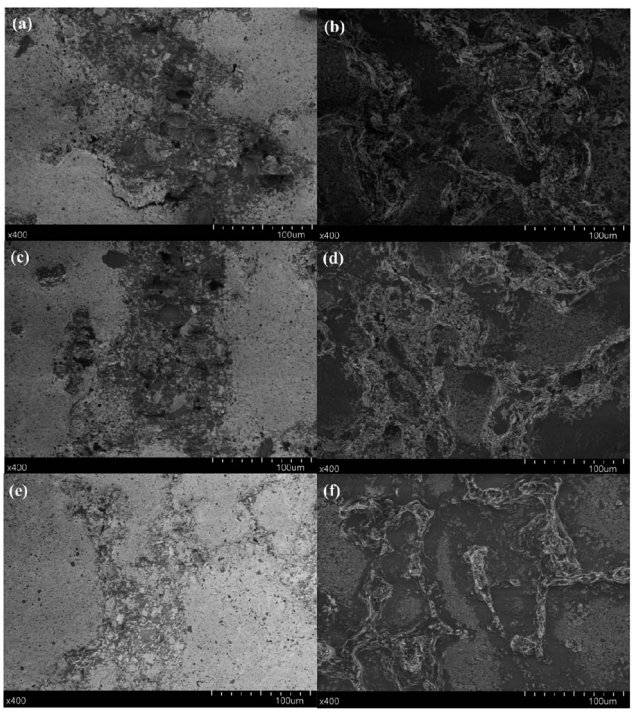

Fig. 9 Surface morphology: (a), (c), and (e) pushed fracture interfaces on glass substrates; (b), (d), and (f) pushed fracture interfaces on glass chips; (a) and (b) were bonded by ECA-80, (c) and (d) by ECA-85, and (e) and (f) by ECA-90.

In short, the sandwiched ECA films were cracked from side to side, from the glass substrate (bonding interface) to the glass chip (bonded interface), to form these surface morphologies. The pushed fracture interfaces on glass chips were much rougher than those on the glass substrates. The surface roughness decreased visually as the weight percentage of silver micro-flakes increased from 80% to 90%. Moreover, solid-to-solid contacts among the glass substrate, ECA, and glass chip increased accordingly as silver micro-flakes increased in the ECAs, which also reduced the mechanical strength. Because of the variations in the surface morphologies, surface roughness, and solid-to-solid contact, the shear strength of the ECAs decreased as the weight percentage of silver micro-flakes increased from 80% to 90% in the ECAs [Fig. 8(a)].

We also used nanoindentation to study the nano-dynamic mechanical properties of the ECAs. The photonically cured ECA-80 at 100 pulses (Fig. S1†) was polished mechanically using an ECOMET 300 variable speed grinder-polisher (Buehler, Lake Bluff, IL, USA). Fig. S5† presents the polished cross-section of the samples. The thickness of the cured ECA film was about 50 μm on the glass substrate. The storage and loss moduli at different depths in the ECA film were obtained using a nanoindentation technique. As shown in Fig. 10(a), the storage modulus at a position of 0–32 μm was for the ECAs, and that at 32–40 μm for the glass substrate. In the range of 0–32 μm, the matrix resin showed a low storage modulus around 7 GPa at positions of 7–14, 16–17, 22–24, and 27–32 μm; other storage modulus peaks in this range were caused by silver micro-flakes [Fig. 10(b)]. Fig. 10(c) shows the loss storage modulus. As with the storage modulus, the silver micro-flakes also caused the loss modulus peaks in the range of 0–32 μm [Fig. 10(d)]; the matrix resin displayed a low loss modulus around 1.9 GPa, and that at 32–40 μm was for the glass substrate. The matrix resin presented the same storage and loss moduli at different positions (or depths), as indicated by the dashed lines marked in Fig. 10(a) and (c). This phenomenon also suggested that these ECAs were crosslinked and cured uniformly at 100 pulses, which coincided well with the FTIR spectra (Fig. 2), double bond conversion (Fig. 3), DSC curves (Fig. 4), and TG-DTA traces (Fig. 5).

Furthermore, the ECAs fabricated in this study were stored at room temperature, avoiding light. There was no gel, separation, delamination, or curing during the storage. They had storage times as long as that of the matrix resin, which were far superior to existing ECA products needing frozen storage. With the ultrafast curing under intense pulsed light, low bulk resistivity, high mechanical strength, long storage time at room temperature, no other additives, and easy use, these ECAs are bound to have a

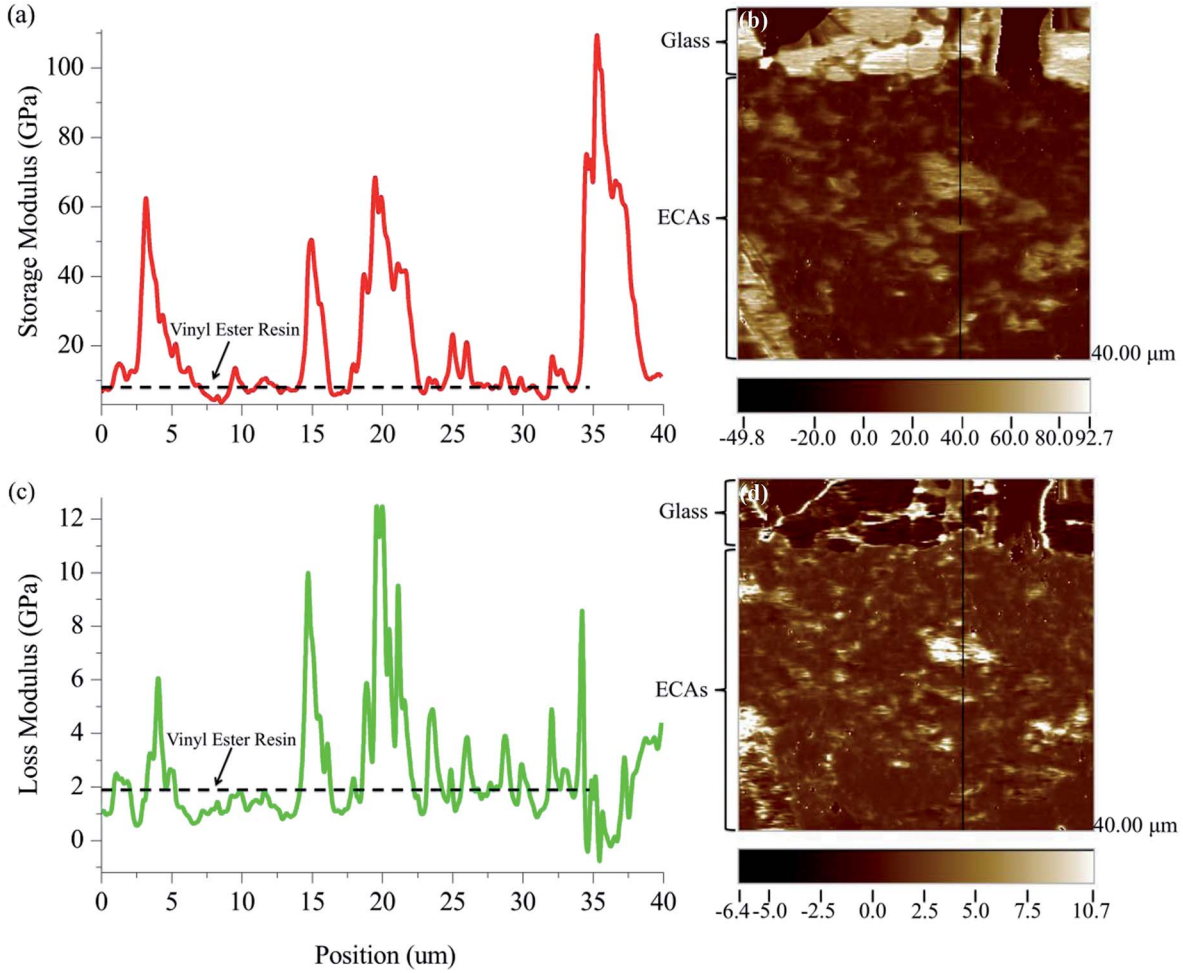

Fig. 10 (a) Storage modulus, (c) loss modulus, (b) and (d) tested cross-sections of photonically cured ECA-80 (100 pulses).

good application prospect in printed electronics, which need low temperature and fast processes.

Conclusions

In this study, we introduced a photonic curing process to cure the ECAs fabricated from a vinyl ester resin and silver micro-flakes. Conventional heat curing at 120–150 °C takes 30–60 min and ultraviolet ray curing takes several to tens of minutes. In contrast, this process can be completed in only 140 ms without any photosensitizers or photoinitiators. The electrically conductive vinyl ester resin–silver flake adhesives absorbed the intense pulsed light and opened the double bonds in the resin, resulting in crosslinking and curing. When the weight percentages of silver micro-flakes were 80%, 85%, and 90% in the ECAs, the bulk resistivity was 1.85×10^{-5}, 1.41×10^{-5}, and 7.54×10^{-6} Ω cm, respectively, and the shear strengths were 6.75, 6.25, and 5.00 MPa, which were good enough for the application of these ECAs in the printed electronics field. These ECAs with low bulk resistivity, high mechanical strengths, and long storage times have been formed using photonic curing at room temperature under an ambient atmosphere, which will be used to manufacture electronic devices in the future.

Acknowledgements

The authors are very grateful to Dr Naoki Fujisawa (Hysitron Inc.) for assistance with nanoindentation measurements.

Notes and references

1 Y. Li, K. S. Moon and C. P. Wong, *Science*, 2005, **308**, 1419–1420.
2 D. Lu and C. P. Wong, Conductive adhesives for flip-chip applications, in *Advanced Flip Chip Packaging*, ed. H. M. Tong, Y. S. Lai and C. P. Wong, Springer, New York, US, 2013, pp. 201–261.
3 L. N. Ho and H. Nishikawa, *J. Electron. Mater.*, 2012, **41**, 2527–2532.
4 X. Y. Zhu, Y. L. Liu, J. M. Long and X. L. Liu, *Rare Met.*, 2012, **31**, 64–70.
5 F. T. Tan, X. L. Qiao, J. G. Chen and H. S. Wang, *Int. J. Adhes. Adhes.*, 2006, **26**, 406–413.
6 H. W. Cui, Q. Fan, D. S. Li and X. Tang, *J. Adhes.*, 2013, **89**, 19–36.
7 X. J. Yang, W. He, S. X. Wang, G. Y. Zhou and Y. Tang, *J. Mater. Sci.: Mater. Electron.*, 2012, **23**, 108–114.

8 G. Y. Si, Y. H. Zhao, J. T. Lv, M. Q. Lu, F. W. Wang, H. L. Liu, N. Xiang, T. J. Huang, A. J. Danner, J. H. Teng and Y. J. Liu, *Nanoscale*, 2013, **5**, 6243–6248.
9 Y. Kwon, B. S. Yim, J. M. Kim and J. Kim, *Microelectron. Reliab.*, 2011, **51**, 812–818.
10 H. W. Cui, A. Kowalczyk, D. S. Li and Q. Fan, *Int. J. Adhes. Adhes.*, 2013, **44**, 220–225.
11 H. W. Cui, D. S. Li and Q. Fan, *Electron. Mater. Lett.*, 2013, **9**, 299–307.
12 Y. Zhang, S. H. Qi, X. M. Wu and G. C. Duan, *Synth. Met.*, 2011, **161**, 516–522.
13 J. Tang, Q. Chen, L. G. Xu, S. Zhang, L. Z. Feng, L. Cheng, H. Xu, Z. Liu and R. Peng, *ACS Appl. Mater. Interfaces*, 2013, **5**, 3867–3874.
14 Z. X. Zhang, X. Y. Chen and F. Xiao, *J. Adhes. Sci. Technol.*, 2011, **25**, 1465–1480.
15 J. T. Jiu, M. Nogi, T. Sugahara, T. Tokuno, T. Araki, N. Komoda, K. Suganuma, H. Uchida and K. Shinozaki, *J. Mater. Chem.*, 2012, **22**, 23561–23567.
16 H. W. Cui, D. S. Li and Q. Fan, *Electron. Mater. Lett.*, 2013, **9**, 1–5.
17 H. W. Cui, D. S. Li, Q. Fan and H. X. Lai, *Int. J. Adhes. Adhes.*, 2013, **44**, 232–236.
18 M. Inoue, H. Muta, S. Yamanaka and K. Suganuma, *J. Electron. Mater.*, 2009, **38**, 2013–2022.
19 Z. Li, K. Hansen, Y. G. Yao, Y. Q. Ma, K. S. Moon and C. P. Wong, *J. Mater. Chem. C*, 2013, **1**, 4368–4374.
20 M. Yoonessi, D. A. Scheiman, M. Dittler, J. A. Peck, J. Ilavskye, J. R. Gaierc and M. A. Meador, *Polymer*, 2013, **54**, 2776–2784.
21 X. H. Zhong, R. Wang and Y. Y. Wen, *Phys. Chem. Chem. Phys.*, 2013, **15**, 3861–3865.
22 Q. Yin, A. J. Li, W. Q. Wang, L. G. Xia and Y. M. Wang, *J. Power Sources*, 2007, **165**, 717–721.
23 N. L. Liu, S. H. Qi, S. S. Li, X. M. Wu and L. M. Wu, *Polym. Test.*, 2011, **30**, 390–396.
24 T. Araki, M. Nogi, K. Suganuma, M. Kogure and O. Kirihara, *IEEE Electron Device Lett.*, 2011, **32**, 1424–1426.
25 T. Araki, T. Sugahara, M. Nogi and K. Suganuma, *Jpn. J. Appl. Phys.*, 2012, **51**, 11PD01.
26 R. Abderrahmen, C. Gavory, D. Chaussy, S. Briançon, H. Fessi and M. N. Belgacem, *Int. J. Adhes. Adhes.*, 2011, **31**, 629–633.
27 Z. Czech, A. Kowalczyk, R. Pełech, R. J. Wróbelb, L. Shao, Y. Bai and J. Świdersk, *Int. J. Adhes. Adhes.*, 2012, **36**, 20–24.
28 H. W. Cui and W. H. Du, *J. Adhes.*, 2013, **89**, 714–726.
29 W. T. Xu and S. W. Rhee, *Org. Electron.*, 2010, **11**, 996–1004.
30 J. C. Zhao, F. P. Du, X. P. Zhou, W. Cui, X. M. Wang, H. Zhu, X. L. Xie and Y. W. Mai, *Composites, Part B*, 2011, **42**, 2111–2116.
31 H. Y. Li, K. S. Moon and C. P. Wong, *J. Electron. Mater.*, 2004, **33**, 106–113.
32 J. Lee, C. S. Cho and J. E. Morris, *Microsyst. Technol.*, 2009, **15**, 145–149.
33 H. W. Cui, D. S. Li and Q. Fan, *Polym. Adv. Technol.*, 2013, **24**, 114–117.
34 H. W. Cui, Q. Fan and D. S. Li, *Polym. Int.*, 2013, **62**, 1644–1651.
35 Y. Li, D. Lu and C. P. Wong, Characterizations of electrically conductive adhesives, in *Electrical Conductive Adhesives with Nanotechnologies*, ed. Y. Li, D. Lu and C. P. Wong, Springer, New York, US, 2010, pp. 81–120.
36 W. T. Cheng, Y. W. Chih and C. W. Lin, *Int. J. Adhes. Adhes.*, 2007, **27**, 236–243.
37 Y. Zhang, S. H. Qi, X. M. Wu and G. C. Duan, *Synth. Met.*, 2011, **161**, 516–522.
38 M. Allen, M. Aronniemi, T. Mattila, A. Alastalo, K. Ojanperä, M. Suhonen and H. Seppä, *Nanotechnology*, 2008, **19**, 175201.
39 J. Leppäniemi, M. Aronniemi, T. Mattila, A. Alastalo, M. Allen and H. Seppä, *IEEE Trans. Electron Devices*, 2011, **58**, 151–159.
40 K. Maekawa, K. Yamasaki, T. Niizeki, M. Mita, Y. Matsuba, N. Terada and H. Saito, *IEEE Trans. Compon., Packag., Manuf. Technol.*, 2012, **2**, 868–877.
41 K. Zimmer, M. Ehrhardt, P. Lorenz, T. Stephan, R. Ebert and A. Braun, *Opt. Laser Technol.*, 2013, **49**, 320–324.
42 J. Perelaer, M. Klokkenburg, C. E. Hendriks and U. S. Schubert, *Adv. Mater.*, 2009, **21**, 4830–4834.
43 J. Perelaer, R. Abbel, S. Wünscher, R. Jani, T. van Lammeren and U. S. Schubert, *Adv. Mater.*, 2012, **24**, 2620–2625.
44 K. A. Schroder, S. C. McCool and W. R. Furlan, *Technical Proceedings of the 2006 NSTI Nanotechnology Conference and Trade Show*, 2006, vol. 3, pp. 198–201.
45 K. A. Schroder, *Technical Proceedings of the 2011 NSTI Nanotechnology Conference and Trade Show*, 2011, vol. 2, pp. 220–223.
46 W. H. Chung, H. J. Hwang, S. H. Lee and H. S. Kim, *Nanotechnology*, 2013, **24**, 035202.
47 S. H. Park, S. Jang, D. J. Lee, J. Oh and H. S. Kim, *J. Micromech. Microeng.*, 2013, **23**, 015013.
48 H. S. Kim, S. R. Dhage, D. E. Shim and H. T. Hahn, *Appl. Phys. A: Mater. Sci. Process.*, 2009, **97**, 791–798.
49 J. S. Kang, J. Ryu, H. S. Kim and H. T. Hahn, *J. Electron. Mater.*, 2011, **40**, 2268–2277.
50 B. Y. Wang, T. H. Yoo, Y. W. Song, D. S. Lim and Y. J. Oh, *ACS Appl. Mater. Interfaces*, 2013, **5**, 4113–4119.
51 Q. J. Mao, L. J. Bian and M. Huang, *J. Polym. Res.*, 2011, **18**, 1751–1756.
52 L. Jin, T. Agag and H. Ishida, *Polym. Int.*, 2013, **62**, 71–78.
53 A. Mautner, X. H. Qin, H. Wutzel, S. C. Ligon, B. Kapeller, D. Moser, G. Russmueller, J. Stampfl and R. Liska, *J. Polym. Sci., Part A: Polym. Chem.*, 2013, **51**, 203–212.
54 J. Z. Y. Wang and R. H. Bogner, *Int. J. Pharm.*, 1995, **113**, 113–122.

